

Optical and near-infrared velocity dispersions of early-type galaxies^{*}

Joachim Vanderbeke^{1,2}, Maarten Baes¹, Aaron J. Romanowsky^{3,4}, Linda Schmidtbreick²

¹ *Sterrenkundig Observatorium, Universiteit Gent, Krijgslaan 281 S9, B-9000 Gent, Belgium*

² *European Southern Observatory, Alonso de Córdova 3107, Vitacura, Santiago, Chile*

³ *UCO/Lick Observatory, University of California, Santa Cruz, CA 95064, USA*

⁴ *Departamento de Astronomía, Universidad de Concepción, Casilla 160-C, Concepción, Chile*

Accepted 2010 November 16. Received 2010 November 15; in original form 2010 August 31

ABSTRACT

We have carried out a systematic, homogeneous comparison of optical and near-infrared dispersions. Our magnitude-limited sample of early-type galaxies in the Fornax cluster comprises 11 elliptical and 11 lenticular galaxies more luminous than $M_B = -17$. We were able to determine the central dispersions based on the near-infrared CO absorption band head for 19 of those galaxies. The velocity dispersions range from less than 70 km s^{-1} to over 400 km s^{-1} . We compare our near-infrared velocity dispersions to the optical dispersions measured by Kuntschner (2000). Contrary to previous studies, we find a one-to-one correspondence with a median fractional difference of 6.4%. We examine the correlation between the relative dust mass and the fractional difference of the velocity dispersions, but find no significant trend. Our results suggest that early-type galaxies are largely optically thin, which is consistent with recent Herschel observations.

Key words: galaxies: clusters: individual: Fornax – galaxies: elliptical and lenticular, cD – galaxies: kinematics and dynamics

1 INTRODUCTION

The dust content of early-type galaxies (ellipticals and lenticulars), and the effects on galaxy parameters inferred from optical observations, is still unclear and a hot topic of debate. Dust in early-type galaxies was first observed in the form of dust lanes and patches (Hawarden et al. 1981; Ebner & Balick 1985; Veron-Cetty & Veron 1988). Later HST observations revealed that dust extinction features exist in a large fraction of early-type galaxies (van Dokkum & Franx 1995). Nonetheless, the optical dust features could not explain the high far-infrared (FIR) fluxes found by Goudfrooij & de Jong (1995) (based on *Infrared Astronomical Satellite* (IRAS) observations). Their results implied dust masses exceeding the values from optical extinction by nearly an order of magnitude, indicating that the major part of the dust is diffusely distributed. Furthermore, the dust mass estimates based on IRAS flux densities are only a lower limit for the true dust masses, because IRAS is not sensitive to cold dust. FIR observations of early-type galaxies selected from the *Infrared Space Observatory* (ISO) archive found that the colder dust component dominates the total dust mass, which is typically more than 10 times larger than the dust masses previously estimated using IRAS observations (Temi et al. 2004). Recent FIR Spitzer observations of elliptical galaxies show evidence of diffuse dust (Temi et al. 2007) and ground-based submillimetre continuum observations with SCUBA have already revealed that galaxies in-

deed contain large amounts of cold dust, but that the submm emission of some of the elliptical galaxies may be synchrotron rather than dust emission (Vlahakis et al. 2005). Nevertheless, the Herschel Space Observatory is crucial for detecting the missing cold dust component and, as a consequence, for making accurate dust estimates in ellipticals (Boselli et al. 2010). Science Demonstration Phase results for the Herschel Virgo Cluster Survey (Davies et al. 2010) did not confirm the diffuse dust thesis in elliptical galaxies: Clemens et al. (2010) found no detection for passively evolving early-type galaxies and Baes et al. (2010) did not find evidence for a diffuse dust component in M87, explaining the FIR emission by a synchrotron model.

The influence of dust on the optical and NIR photometry of early-type galaxies was studied by Michard (2005) and models to predict the effect of dust were developed by Witt et al. (1992) and Wise & Silva (1996, 1997). Baes & Dejonghe (2000, 2001, 2002) and Baes et al. (2000) were the first to include the influence of dust on the observed stellar kinematics in their models. They showed that dust may bias optical observations through absorption and scattering, thus influencing the photometric and kinematic data. Such effects would have widespread ramifications for studies of early-type galaxies, as velocity dispersions play a significant role in tracking the mass evolution of early-type galaxies (van der Marel & van Dokkum 2007), and appear in empirical relationships such as the the $M_{\text{BH}}-\sigma$ relation (Ferrarese & Merritt 2000; Gebhardt et al. 2000; Graham 2008; Gültekin et al. 2009; Kormendy & Bender 2009; Graham et al. 2010), the Faber-Jackson relation and the Fundamental Plane relation (Djorgovski & Davis

^{*} Based on new observations collected at the European Southern Observatory, Cerro Paranal, Chile; ESO program 082.B-0897A.

1987; Dressler et al. 1987; Guzman et al. 1993; Pahre et al. 1995; Prugniel & Simien 1996; Graham & Colless 1997; Gavazzi et al. 1999; Bernardi et al. 2003; Michard & Prugniel 2004; Desroches et al. 2007; Fraix-Burnet et al. 2010; Ribeiro & Dantas 2010).

One way to investigate the effect of dust on the kinematics is to compare the optical and NIR velocity dispersions. The K -band is the optimal region to perform a study on NIR velocity dispersions: the extinction by dust in the K -band is only 7% of that in the B -band (where dust is very opaque) and the wavelengths are short enough to evade dilution of the stellar continuum by hot dust (Gaffney et al. 1995). In the K -band, one can use the $2.29\ \mu\text{m}$ ($2-0$) ^{12}CO absorption band head as a kinematical tracer. It is the strongest absorption feature in galactic spectra in the $1-3\ \mu\text{m}$ range and increases in strength with decreasing effective temperature or increasing radius of the underlying stars (Silge & Gebhardt 2003). This late-type star feature can be used to probe the kinematics of the red stellar population of galaxies (Gaffney et al. 1993) and is intrinsically sharp and deep, spectrally isolated from other strong absorption and emission features and is located in a dark part of the infrared sky spectrum (Lester & Gaffney 1994). The advent of efficient NIR spectrographs and detectors on large telescopes has made the CO absorption band a generally available tool for kinematic studies (e.g. Silge et al. 2005; Nowak et al. 2007, 2008; Lyubenova et al. 2008).

Comparative studies about NIR and optical velocity dispersions were performed in the past. Silge & Gebhardt (2003) were the first to perform a systematic study, but their sample was biased to lenticulars (it contained 25 galaxies, of which 7 ellipticals and 18 lenticulars) and was based on inhomogeneous optical velocity dispersions, obtained from different papers with different instruments, methods and extraction windows. They found that the velocity dispersion decreases with wavelength, opposite to the theoretical expectations of Baes & Dejonghe (2002). Silva et al. (2008) studied the stellar populations in early-type galaxies, using the strong spectral features near $2.2\ \mu\text{m}$. They found a one-to-one correspondence between the optical and NIR velocity dispersions, based on a homogeneous set of 4 lenticular and 7 elliptical galaxies. 10 out of the 11 galaxies are part of our new, extended sample, in which we excluded NGC 1344, because this galaxy was not included in the sample of Kuntschner (2000). Rothberg & Fischer (2010) inspected the NIR and optical velocity dispersions in infrared-luminous mergers. Their reference sample of elliptical galaxies did not show much evidence for a σ -discrepancy, but they found a strong correlation with IR-luminosity and dust masses in merging galaxies.

To investigate the disagreement between the different velocity dispersion studies, we embarked on a project, for the first time using a complete and well-balanced sample of 22 early-type galaxies (comprising 11 ellipticals and 11 lenticulars). All galaxies are members of the Fornax cluster, the nearest galaxy cluster after the Virgo cluster. Fornax is considerably more compact and regular in shape than Virgo, doubling the central density of galaxies but having a total mass of nearly an order of magnitude lower. This makes the Fornax cluster a good representative of the groups and poor clusters in which most galaxies in the universe reside (Jordán et al. 2007). Nevertheless, the main reason for the choice of our sample was the availability of uniform spectroscopic optical data, obtained by Kuntschner (2000). In his paper, velocity dispersion, age, metallicity and line strength are discussed for all galaxies in the sample.

This paper is organized as follows: § 2 presents the data and the data reduction, § 3 presents the comparison of the optical and IR velocity dispersions and the relation with the dust mass. In § 4 our conclusions are presented.

2 OBSERVATIONS AND DATA REDUCTION

2.1 Data sample

This study is based on the complete magnitude-limited sample of Kuntschner (2000). This sample, presented in Table 1, has been selected from the catalogue of Fornax galaxies of Ferguson (1989), in order to obtain a complete sample down to $B_T = 14.2$ or $M_B = -17$ and contains 11 elliptical and 11 lenticular galaxies. Recent measurements of B_T were taken from the NASA/IPAC Extragalactic Database.

2.2 Observations

The observations were performed between 20 October 2008 and 26 January 2009 with the VLT using the SW arm of ISAAC (Moorwood et al. 1998) in spectroscopic medium resolution mode (SWS-MR). The characteristics of the detector and the instrumental set-up are given in Table 2.

We used the nod-on-slit mode (double subtraction technique). Every observational sequence was started with the galaxy centered on the slit near one end and an individual spectrum was taken. The galaxy was then moved $60''$ or $90''$ towards the other end of the slit and two more integrations were executed. Then the galaxy was placed again at the original slit position where another spectrum was taken. This ABBA sequence was repeated a number of times, resulting in multiple individual two-dimensional spectroscopic images. In order to remove properly the sky background for the observations of big and bright galaxies (i.e. for NGC 1399, NGC 1316, NGC 1380, NGC 1404 and NGC 1427 in particular), we observed separate sky spectra. That way, only half of the frames contained the galaxy spectrum, resulting in an observing sequence of the form OSSO (O=object integration, S=sky integration). Total on source exposure times were between 900 and 2400s [see Table 1 for a detailed listing, with '(1/2)' denoting OSSO observations]. The seeing was generally sub-arcsecond, reaching as low as $\sim 0.5''$ in the best cases.

To be able to remove the telluric lines, we observed B-type standard stars with the same observing sequence we have used for our science targets. These hot stars do not have any spectral features in the wavelength interval we are considering. Moreover, their continuum in the K -band is well approximated by the Rayleigh-Jeans part of the blackbody spectrum (Silva et al. 2008). To remove the stellar signature, we divide the spectrum by a template of the corresponding type of star (Pickles 1998). All the remaining variation in the spectra is due to observational features and is caused by the telluric lines and the instrument response, so, by dividing the galaxy spectra by this residual template spectrum, we remove the telluric lines and the detector signature. Because of the variability of the NIR sky, we impose the conditions that the difference in observing time between the target and the standard star has to be less than 2 hours and that the difference in airmass between the observations has to be less than 0.2.

2.3 Data reduction

The basic data reduction steps were performed with the ISAAC pipeline and MIDAS. The sky subtraction, bias subtraction, flat fielding and wavelength calibration (based on the OH-lines) were done by the ISAAC pipeline. The removal of telluric lines (using our standard star observations) was done with MIDAS. If possible and appropriate, we increased the S/N of the telluric profile by

Table 1. Galaxy sample.

Galaxy	Type	B_T [mag]	Exposure time [s]	PA [°]	σ_{opt} [km s ⁻¹]	σ_{NIR} [km s ⁻¹]	$\sigma_{\text{NIR},23 \text{ templates}}$ [km s ⁻¹]	EW _{CO} [Å]	S/N
NGC 1316	S0 pec	9.4	1800 (1/2)	47	221.0 ± 11.0	237.7 ± 11.1	218.6 ± 9.9	13.56	89
NGC 1336	E4	13.1	2400	10	96.0 ± 5.0	119.0 ± 8.2	126.9 ± 7.0	13.04	66
NGC 1339	E5	12.5	1200	159	158.0 ± 8.0	182.4 ± 9.2	175.2 ± 9.4	14.41	57
NGC 1351	E5	12.5	1200	140	157.0 ± 8.0	153.0 ± 6.6	148.4 ± 5.5	9.58	73
NGC 1373	E3	14.1	2400	130	75.0 ± 4.0	79.8 ± 4.7	72.5 ± 4.0	11.26	66
NGC 1374	E0	12.0	1200	120	185.0 ± 9.0	206.8 ± 10.0	193.9 ± 9.7	13.72	72
NGC 1375	S0	13.2	1800	90	56.0 ± 10.0	64.1 ± 4.2	58.2 ± 3.8	11.66	68
NGC 1379	E0	11.8	1200	65	130.0 ± 7.0	130.0 ± 6.8	123.3 ± 5.3	12.02	90
NGC 1380	S0	10.9	1800 (1/2)	7	219.0 ± 11.0	189.8 ± 16.6	199.8 ± 20.8	12.19	59
NGC 1380A	S0	13.3	2400	178	55.0 ± 9.0	59.9 ± 9.1	51.2 ± 8.6	11.41	33
NGC 1381	S0	12.4	1200	139	153.0 ± 8.0	155.2 ± 5.7	148.3 ± 4.6	11.70	129
NGC 1399	E0, cD	10.6	1800 (1/2)	175	375.0 ± 19.0	405.5 ± 33.1	409.0 ± 34.2	11.87	40
NGC 1404	E2	11.0	1800 (1/2)	163	260.0 ± 13.0	246.9 ± 21.6	240.9 ± 19.0	13.30	84
NGC 1419	E0	13.5	2400	125	117.0 ± 6.0	125.4 ± 5.0	119.2 ± 3.7	10.45	108
NGC 1427	E4	11.8	1800 (1/2)	76	175.0 ± 9.0	154.9 ± 17.5	150.3 ± 14.6	9.87	62
IC 1963	S0	12.9	2400	83	58.0 ± 10.0	48.6 ± 5.6	40.3 ± 4.7	9.97	57
IC 2006	E	12.2	1800	10	136.0 ± 7.0	125.4 ± 10.2	118.7 ± 8.1	14.18	50
ESO 359-G02	S0	14.2	1800	50	45.0 ± 8.0	7
ESO 358-G06	S0	13.9	1800	31	57.9 ± 10.8	55.1 ± 25.0	52.8 ± 24.8	13.20	13
ESO 358-G25	S0 pec	13.8	1800	60	58.0 ± 10.0	8
ESO 358-G50	S0	13.9	1800	172	49.0 ± 8.0	17
ESO 358-G59	S0	14.0	1800	160	54.0 ± 9.0	70.0 ± 20.4	65.0 ± 14.9	10.83	29

Notes.-Morphological type and optical velocity dispersions taken from Kuntschner (2000), B_T from NASA/IPAC Extragalactic Database. Empirical S/N estimates were determined for the extracted spectra as described in §2.3.

Table 2. The instrumental set-up.

Telescope	VLT UT1/Antu
Dates	20 October 2008 - 26 January 2009
Instrument	ISAAC
Spectral range	0.98 – 2.5 μm
Grating	MR
Dispersion	1.22 Å pixel ⁻¹
Resolution (FWHM)	8.196 Å
Spatial Scale	0.1484 arcsec pixel ⁻¹
Slit Width	1 arcsec
Detector	Hawaii
Gain	4.6 e ⁻ ADU ⁻¹
Read-out noise	~ 10 e ⁻
Seeing	< 1''
Pixel Size	18.5 μm

averaging different observations of telluric stars. For NGC 1380, telluric lines have not been removed, because of a problem with the wavelength calibration of the standard star. For all spectra we had some problem around 2.3 μm to correct a telluric absorption line with a very sharp edge. As a result, a spike-like emission feature remains in the corrected spectra. We choose not to remove cosmic rays, but will ignore any contaminated pixel when fitting the stellar template. An average of the 25 central rows was taken to obtain an effective aperture of $1 \times 3.7 \text{ arcsec}^2$, choosing a slit width of 1 arcsec to obtain the needed spectral resolution and approximating the spatial width of the $2.3 \times 3.85 \text{ arcsec}^2$ optical aperture used by Kuntschner (2000). We do not increase the extraction width to obtain a better S/N, because the velocity dispersion can be strongly aperture-dependent (as shown in Fig. 1), and it is important to be well-matched to Kuntschner (2000). As a final step, the spectra were rebinned to a common wavelength increment (2.43 Å/pix),

approximately doubling the original step size. To illustrate the effect of the different data reduction steps, we refer to Fig. 2, where a central 3.7'' extraction of NCG 1381 is shown for the different data reduction steps: the ISAAC pipeline result, after removing the telluric lines and after rebinning to the 2.43 Å/pix wavelength increment. For each extracted spectrum, we have derived an empirical S/N following the method described by Stoehr et al. (2007). The resulting S/N per rebinned element ranges from ~ 7 for the faintest galaxies to more than 100 for the brightest ones and is listed in Table 1.

The instrumental set-up, as described in Table 2, gives a FWHM resolution of approximately 107 km s⁻¹, producing an instrumental contribution to the dispersion of ~ 45 km s⁻¹.

2.4 Velocity dispersion determination

The sharp blue edge of the CO band head allows us to measure the kinematics accurately (Silge & Gebhardt 2003). There are several techniques to obtain the internal kinematical information, e.g. the Fourier correlation quotient (FCQ) method, developed by Bender et al. (1994) and used by Kuntschner (2000). We use the pPXF technique developed by Cappellari & Emsellem (2004). This method rebins the spectrum logarithmically and fits it directly in pixel space. We correct the template continuum shape using additive second degree Legendre polynomials and use a pure Gaussian to model the LOSVD. An alternative LOSVD is inspected in § 3.2, where Gauss-Hermite coefficients h_3 and h_4 are included to model the LOSVD. We apply pPXF to a wavelength range of ~ 2.23 – 2.345 μm , fitting not only the CO band head, but also including a part of the spectrum bluewards of it. To illustrate the effect of the velocity dispersion on the CO band head, we refer to Fig. 2 of Silge & Gebhardt (2003).

The choice of the template stars, which we obtained from the

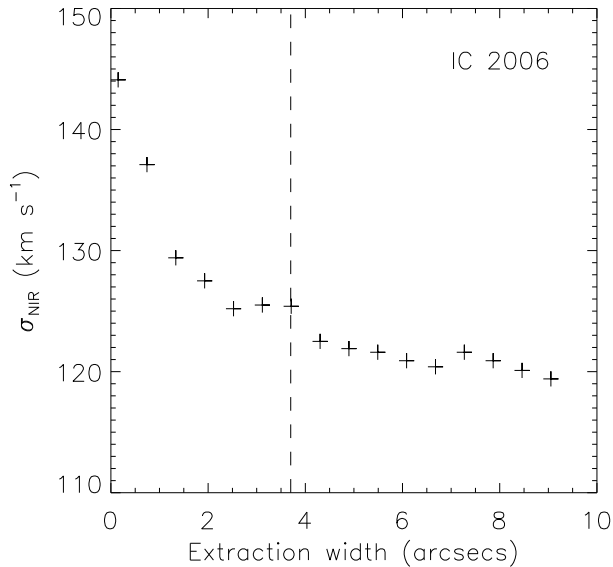


Figure 1. Central velocity dispersion of IC 2006 as a function of the extraction width. The dashed line shows the standard extraction aperture of 3.7 arcsecs.

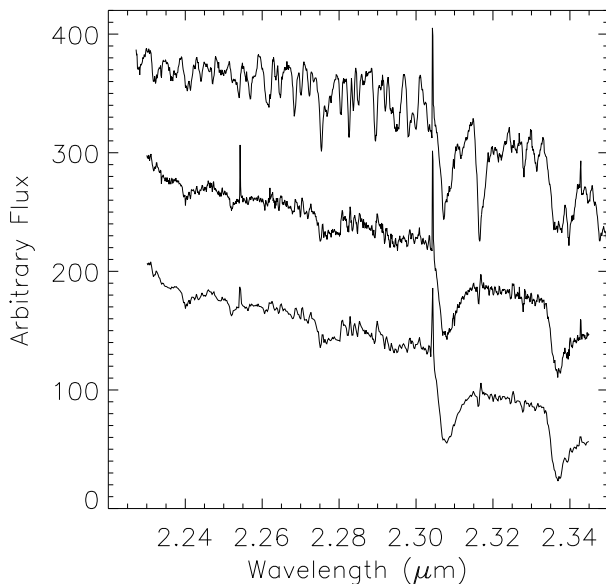


Figure 2. Data reduction steps applied to a central 3.7'' extraction of NGC 1381 are shown (from top to bottom) before corrections for telluric absorption (the pipeline result), after correction for telluric absorption and instrument sensitivity and after rebinning to $\sim 2.43\text{\AA}/\text{pix}$. The sharp emission feature around $2.3\ \mu\text{m}$ is a remnant of the telluric correction. No correction for redshift has been applied. The middle and the bottom spectra have been separated by an arbitrary additive offset; otherwise, they would be on top of each other.

GNIRS and NIFS libraries (Winge et al. 2009), is an important aspect when determining the velocity dispersion: Silge & Gebhardt (2003) showed that the equivalent width of the template used for the fit is important, not the details of the spectral type. To account for the spectral resolution differences between ISAAC and the template libraries, we have logarithmically rebinned the latter to the same velocity scale as the ISAAC spectra, under the assumption that the shape of the instrumental spectral profiles can be well ap-

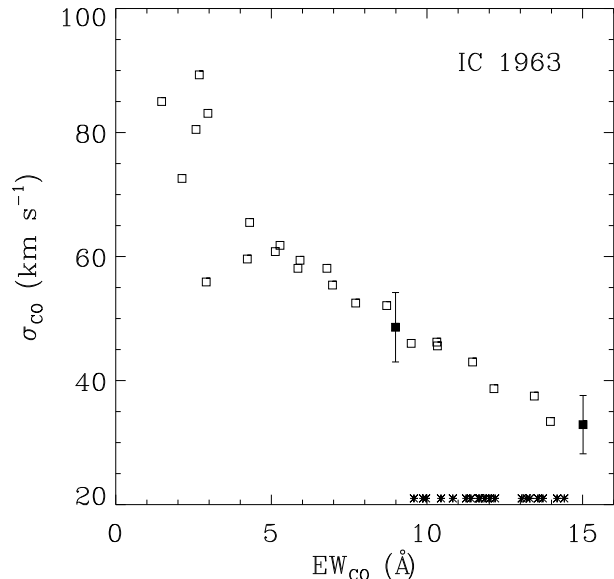


Figure 3. Dispersion measured by the pPXF method for IC 1963 as a function of the equivalent width of the input template. The two filled squares are the results for an average template of K giants ($\text{EW}_{\text{CO}} = 8.99$, $\sigma_0 = 48.6 \pm 5.6$) and M giants ($\text{EW}_{\text{CO}} = 15.01$, $\sigma_0 = 32.9 \pm 4.7$). The asterisks represent the EWs of the galaxies in the sample.

proximated by a Gaussian. Fig. 3 presents the measured central velocity dispersion as a function of the equivalent width of the input template, with equivalent widths ranging from ~ 1.5 to ~ 15 . One concludes that the larger the EW of the CO band of the template, the lower the resulting velocity dispersion required to reproduce the galaxy spectrum. The relative values of the velocity dispersion are only comparable, if a fixed template is used to generate the fits. The filled squares are the results for an average template of K giants (HD206067, HD218594, HD39425 and HD4730 from the GNIRS library) and M giants (HD27796, HD30354, HD23574, HD234791 from the NIFS library). To be consistent with Kuntschner (2000), we choose the average K giant spectrum to fit the galaxy spectra in a homogeneous way. An alternative template scheme is explored in § 3.2, where velocity dispersions have been determined using all the templates of Fig. 3 as input templates for pPXF. The asterisks in Fig. 3 represent the EWs of the galaxies in the sample, given in Table 1. This shows that the stellar library spans the range of the observed CO strength in the galaxies.

Table 1 presents the resulting NIR velocity dispersion σ_{NIR} and the optical velocity dispersions σ_{opt} taken from Kuntschner (2000). The optical velocity dispersions have been used as the initial value in the pPXF method. After trying several approaches, we have used a bootstrap method to estimate the uncertainties on the velocity dispersions, resampling the residuals of the initial fit. For ESO 359-G02, ESO 358-G25 and ESO 358-G50 we did not get a reliable fit, as a consequence of the low S/N for these galaxies and the low expected velocity dispersions (based on the optical values). We decided to exclude these galaxies from the sample. After all, their optical velocity dispersions are not reliable either; they suffered an instrumental broadening of $\sim 105\ \text{km s}^{-1}$, which introduces optical systematic errors for $\sigma < 90\ \text{km s}^{-1}$ [as stated in Kuntschner (2000)].

The spectral fits are presented in Figs. 4 and 5: the thick smooth line is the resulting fit, the thin noisy line represents the galaxy spectrum. Cosmic rays, sharp features and poorly removed

telluric features were flagged as bad pixels and were not used by the pPXF method to generate the fit. If we estimate the error on the fit by the dispersion of the residuals, we obtain $\chi^2/DOF < 1$ for all galaxies, which indicates that we obtain good fits.

3 RESULTS AND DISCUSSION

3.1 Comparing NIR velocity dispersions

The line strength study of Silva et al. (2008) had 4 S0 and 6 E galaxies in common with our galaxy sample [of which 8 are observed with ISAAC and 2 (NGC 1316 and NGC 1399) with SINFONI at the VLT]. For their ISAAC observations in SWS-MR mode, they also used a $120'' \times 1''$ slit and had total exposure times of 3000s or 3200s. This resulted in extracted spectra with a S/N ranging from 48 to 280, based on the S/N determination of Stoehr et al. (2007). However, they applied a procedure derived from the processing of optical long-slit spectra and did not use a simple AB subtraction, because this could cause inaccurate dark and background correction in the lower surface brightness parts of the luminosity profiles. They periodically observed velocity template standard stars, covering the range K5 III to M1 III. Those templates were fitted to the galaxy spectra applying the pPXF method, extracting the NIR velocity dispersions $\sigma_{\text{NIR,Silva}}$. Unfortunately, no uncertainties on the velocity dispersions were given. They used $1'' \times 1/8R_e$ for the extraction window, which results in spatial widths ranging from 0.15 to 0.61 arcsec (extracted R_e for NGC 1404 equals 2.9 arcsecs, kindly provided by Dr. Kuntschner, private communication). For the SINFONI observations, Silva et al. (2008) extracted a slit of $2'' \times 3''$ from the data cube.

In Fig. 1 it is shown that the velocity dispersion can depend on the extraction width. In order to compare our measurements with Silva et al. (2008), we have redetermined the velocity dispersion for the 10 galaxies in common, adopting an extraction width of $1'' \times 1/8R_e$ ($1'' \times 3''$ for NGC 1316 and NGC 1399) and fitting the average K giant template to the galaxy spectra. The measurements are denoted as $\sigma_{\text{NIR},1/8R_e}$. The results are presented in Fig. 6, where the derived velocity dispersions $\sigma_{\text{NIR},1/8R_e}$ are compared to the values $\sigma_{\text{NIR,Silva}}$, derived by Silva et al. (2008). In this and following figures, true elliptical galaxies are represented as open triangles, lenticular galaxies as filled circles. However, to distinguish the 2 galaxies observed with SINFONI by Silva et al. (2008), we have marked those galaxies with asterisks in Fig. 6. We have used the uncertainties on σ_{NIR} as an estimate for the uncertainties on $\sigma_{\text{NIR},1/8R_e}$. The best-fitting line, which is given by

$$\sigma_{\text{NIR},1/8R_e} = (1.04 \pm 0.05)\sigma_{\text{NIR,Silva}} - (13.78 \pm 9.52), \quad (1)$$

has a slope consistent with 1, an intercept marginally inconsistent with 0 and a reduced χ^2 of 1.89. Using the velocity dispersions obtained with the fixed extraction width of $3.7''$ (σ_{NIR}) instead of $\sigma_{\text{NIR},1/8R_e}$ does not change the fit significantly. Thus, our NIR results generally compare well to those of Silva et al. (2008) for the same galaxies.

3.2 Comparing NIR and optical dispersions

Fig. 7 presents the correlation between the optical and NIR central velocity dispersions for 19 galaxies of our sample. The solid line

$$\sigma_{\text{opt}} = (0.99 \pm 0.06)\sigma_{\text{NIR}} - (3.76 \pm 8.72) \quad (2)$$

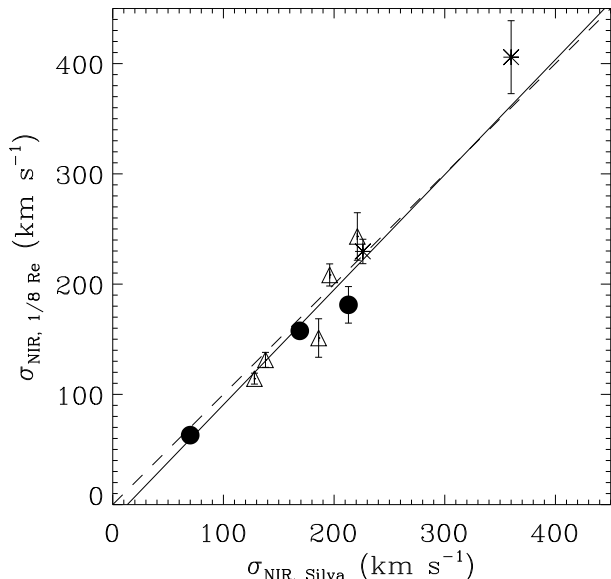


Figure 6. Correlation between the velocity dispersions determined with an extraction window of $1/8 R_e$ and the NIR velocity dispersions from the literature (Silva et al. 2008). The dashed line has a slope of unity, the solid line is the best fit, given by equation 1. Here and in the following plots, the filled circles are S0 galaxies, while the open triangles are E galaxies. The two galaxies observed with SINFONI (Silva et al. 2008) are represented with an asterisk.

shows the best fit, with a slope consistent with 1, an intercept consistent with 0 and a reduced χ^2 of 1.09. The absence of a σ -discrepancy confirms the findings by Silva et al. (2008) and further generalizes their results due to the statistical completeness of this study, but does not agree with Silge & Gebhardt (2003). Their best-fitting line had a slope of 1.189 ± 0.084 and an intercept of -8.6 ± 12.4 .

Kuntschner (2000) had difficulties in determining the velocity dispersions for galaxies with $\sigma_{\text{opt}} < 70 \text{ km s}^{-1}$ and noted that the results of $\sim 50 - 60 \text{ km s}^{-1}$ are only rough estimates. However, excluding the galaxies with $\sigma_{\text{opt}} < 70 \text{ km s}^{-1}$ does not change the results significantly.

Fig. 8 presents a histogram of the fractional difference between NIR and optical measurements of dispersion. The median fractional difference between the optical and the NIR velocity dispersions is 6.4%, the mean fractional difference is 3.9%. Silge & Gebhardt (2003) found a median difference of -11% , opposite to theoretical expectations (Baes & Dejonghe 2002) and to our results.

It is not immediately clear why Silge & Gebhardt (2003) found that NIR velocity dispersion measurements are lower than optical dispersion measurements. One possible reason could be the different spatial range used by Silge & Gebhardt (2003): Fig. 1 indicates that velocity dispersions can decrease for higher spatial ranges. The average spatial width in Silge & Gebhardt (2003) is $\sim 12''$, which may be the reason for their difference between NIR and optical velocity dispersions. In order to investigate this possibility, we recalculated the NIR velocity dispersions for all galaxies in our sample, now using an extraction window of $1'' \times 12''$. The best-fitting line, with a reduced χ^2 of 1.35, is

$$\sigma_{\text{opt}} = (1.03 \pm 0.07)\sigma_{\text{NIR},1 \times 12 \text{arcsec}^2} - (3.35 \pm 9.16), \quad (3)$$

fully consistent with Eq. 2. Fig. 1 suggests an increase of the slope of $\sim 4\%$, which is indeed what we find. Nonetheless, a $\sim 20\%$ effect is needed to explain the results found by Silge & Gebhardt

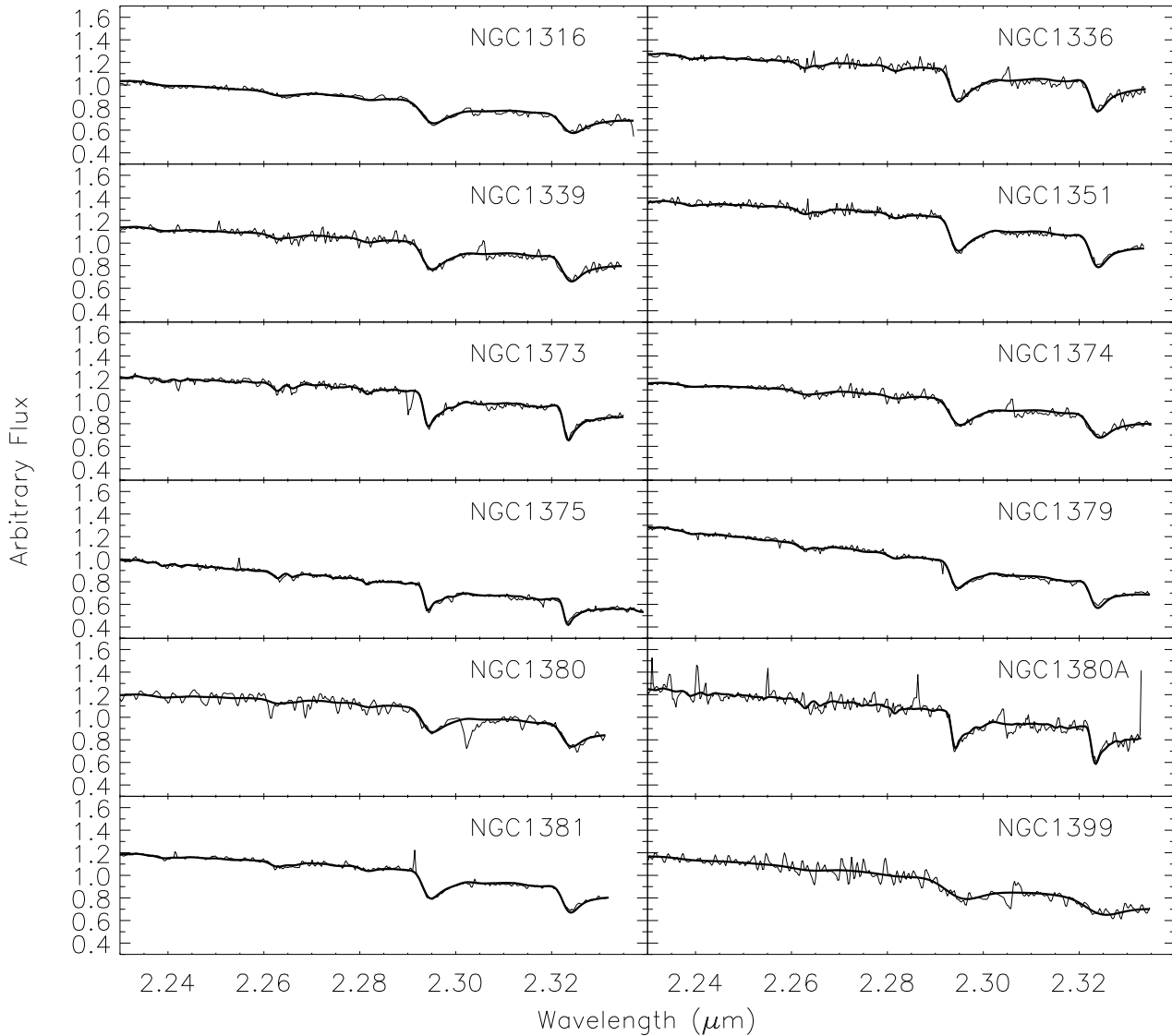


Figure 4. Rest-frame spectra of galaxies (noisy thin curves) and spectra of the average KIII stellar spectrum convolved with the derived velocity distribution (smooth thick curves). Cosmic rays and poorly removed telluric features were flagged as bad pixels and not used to generate the fit. No removal of telluric lines was done for NGC 1380.

(2003), so we exclude that the extraction width is responsible for the discrepancy.

Another possible explanation for the discrepancy could be the choice of the templates: Fig. 3 showed that the measured velocity dispersion depends strongly on the equivalent width of the CO band of the template. Silge & Gebhardt (2003) used templates with equivalent widths ranging from less than 5 to over 20 Å. So far, we have only used the average K giant template with an equivalent width of 8.99 Å. In order to investigate this possibility, we have provided the 23 templates we have used in Fig. 3 as input templates for pPXF. The resulting velocity dispersions are given in Table 1. For every galaxy separately, pPXF gives weights to the different templates to obtain the best fit, delivering stellar population information. pPXF favoured HD113538 (KV), HD2490 (MIII) and HD63425B (KIII), which indicates that the light is dominated by cool giants and dwarfs. The best linear fit is given by

$$\sigma_{\text{opt}} = (0.99 \pm 0.07)\sigma_{\text{NIR,23 templates}} + (2.92 \pm 9.05) \quad (4)$$

and has a reduced χ^2 of 1.70. It is fully consistent with equation

2, indicating that template mismatch does not affect our velocity dispersion determination.

Silge & Gebhardt (2003) used a nonparametric LOSVD. To investigate whether this could account for the discrepancy, we included the h_3 and h_4 Gauss-Hermite coefficients, using the average K giant template as input spectrum and the default pPXF parameter λ to penalize both parameters. The resulting values for h_3 (and h_4) are between -0.05 and 0.11 (-0.01 and 0.08 , respectively) with a median value of 0.012 (0.020 , respectively). The best-fitting line is given by

$$\sigma_{\text{opt}} = (0.99 \pm 0.05)\sigma_{\text{NIR,G-H}} - (2.40 \pm 7.58) \quad (5)$$

with a reduced χ^2 of 0.93. Again, the slope is consistent with 1 and the intercept is consistent with 0, so we exclude that the parametrization of the LOSVD is accountable for the discrepancy.

One remaining possibility for the difference between our results and Silge & Gebhardt (2003) is that the sample selection is important. Our Fornax sample represents only a cluster environment, while the Silge & Gebhardt (2003) sample ranges from cluster to

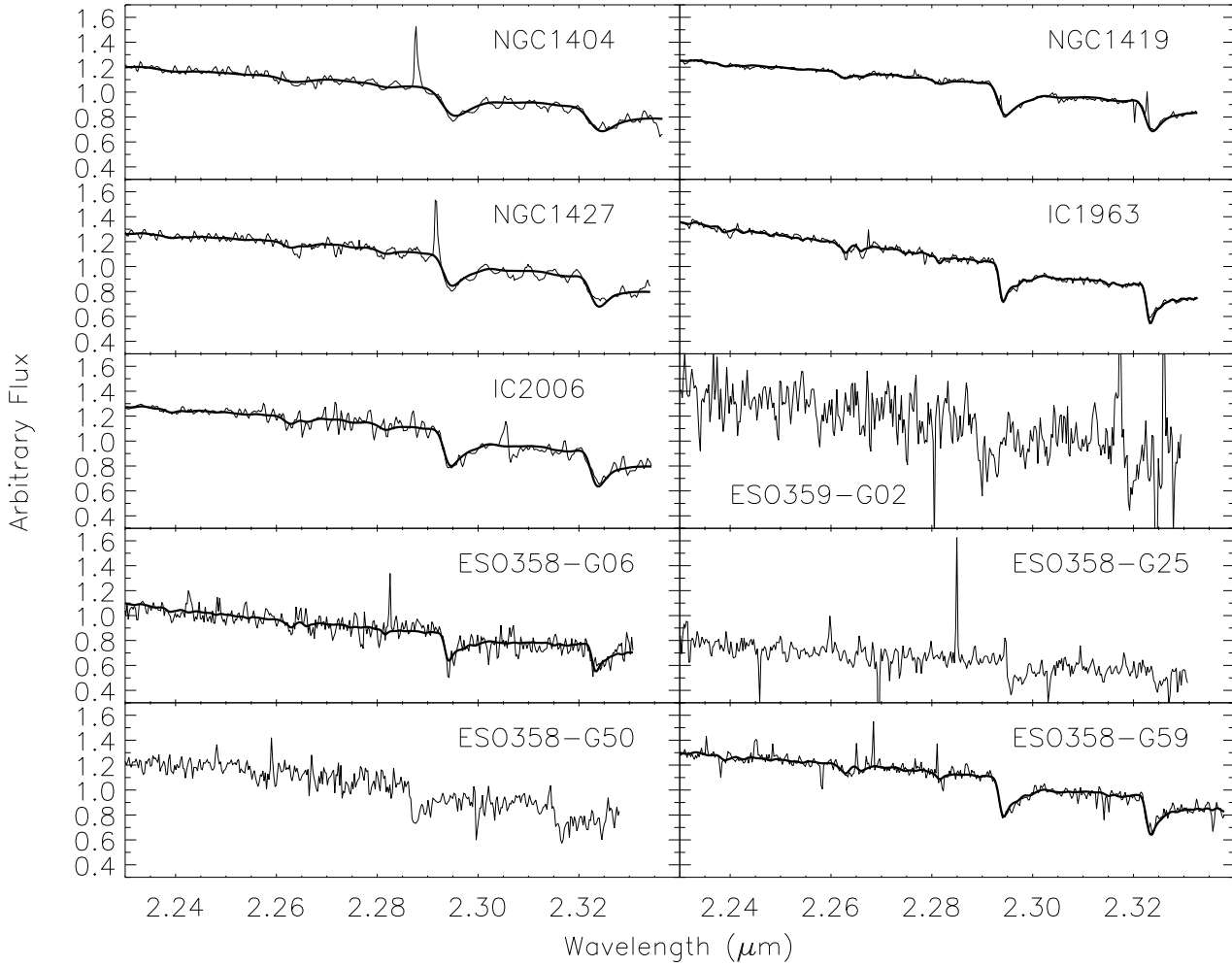


Figure 5. Same as in Fig. 4.

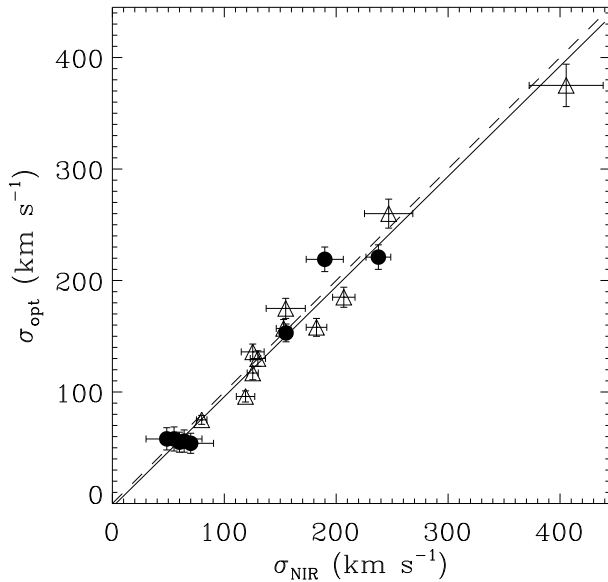


Figure 7. Correlation between the dispersion measured from the CO band head and the optical dispersion (Kuntschner 2000). The dashed line shows where two measurements are equal, the solid line is the best-fitting line, given by equation 2.

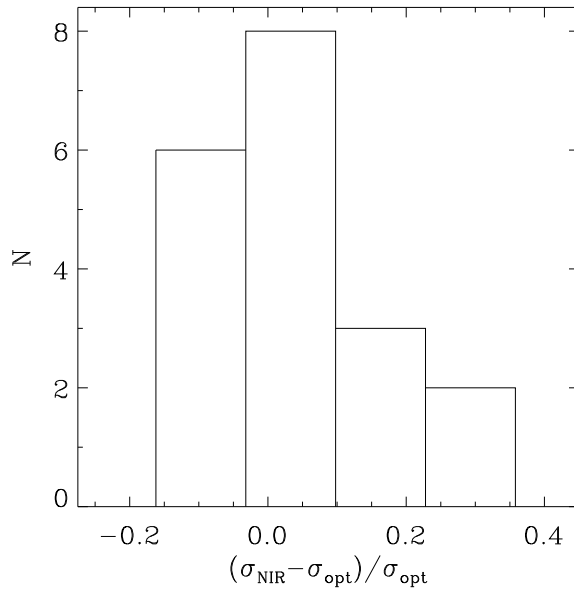


Figure 8. Histogram showing the number of galaxies in each bin of fractional difference between infrared and optical measurements. The median fractional difference is 6.4%, the mean fractional difference is 3.9%.

isolated field galaxies and there are known correlations between environment and velocity dispersion (e.g. Zhu et al. 2010; La Barbera et al. 2010).

3.3 Correlation with IRAS dust masses

According to Silva et al. (2008), at least two galaxies (NGC 1316 and NGC 1380) from our sample show clear central dust features. We need to know how much dust there is in the galaxies to study the effects of dust on the observed kinematics. In this section, we derive the dust masses (M_d) for our galaxies based on IRAS flux densities at 60 and 100 μm . We apply the technique of Goudfrooij & de Jong (1995), using a distance $D = 19.3$ Mpc for all galaxies (Jordán et al. 2007). For 5 galaxies of our sample, both S_{60} and S_{100} were given. In that case both T_d and M_d were determined. If only S_{100} was given, which was the case for 5 galaxies of our sample, we used the average dust temperature $\bar{T}_d = 25.9\text{K}$ of our galaxy sample as a representative value to compute the dust mass. Table 3 presents the resulting dust masses M_d , T_d and the IRAS flux densities for 10 galaxies in our sample. For six galaxies (NGC 1374, NGC 1375, NGC 1381, NGC 1419, NGC 1427, ESO 358-G06) the IRAS Faint Source Catalog lists only upper limits, the three remaining galaxies (NGC 1373, NGC 1380A, IC 1963) are not listed in the catalog.

Fig. 9 presents the fractional difference of the infrared and the optical dispersions as a function of the relative amount of dust in a galaxy, which is estimated in Silge & Gebhardt (2003) by the ratio of the IRAS dust mass to the B -band luminosity. The estimates for the relative amount of dust are given in Table 3. Note that the IRAS dust mass estimates are a lower limit for the true dust masses, because IRAS is not sensitive to cold dust (which emits the bulk of its radiation longwards of 100 μm). A negligible trend is visible (confirmed by the Spearman rank-order correlation coefficient equal to 0.21). The best-fitting solid line is given by equation

$$\frac{\sigma_{\text{NIR}} - \sigma_{\text{opt}}}{\sigma_{\text{opt}}} = (0.008 \pm 0.056) \log\left(\frac{M_d}{L_B}\right) + (0.068 \pm 0.266), \quad (6)$$

with both the slope and the intercept consistent with 0 and a reduced χ^2 of 1.76. This implies that warm dust does not affect optical dispersions. We cannot yet make the same conclusion for colder dust, but Fig. 7 indicates that the typical effect is very weak.

4 CONCLUSIONS

In this study, we investigate a complete magnitude-limited and unbiased sample of 22 early-type galaxies in the Fornax cluster and are able to determine the kinematics based on the $2.29\mu\text{m}$ $^{12}\text{CO}(2-0)$ feature for 19 of those galaxies. We related the NIR velocity dispersions with the optical dispersions of Kuntschner (2000) and found no evidence for a σ -discrepancy for the ellipticals nor for the lenticulars. Our results agree with a previous smaller study of Silva et al. (2008), but not with Silge & Gebhardt (2003). We investigated this disagreement by providing a variety of input templates to pPXF with a large range of EWs, by changing the spatial width of the extraction window and by introducing Gauss-Hermite coefficients in the LOSVD, but we were not able to clarify this discrepancy.

We have computed the dust masses based on IRAS flux densities for 10 galaxies of our sample and investigated the influence of diffuse dust on the observed kinematics, which turned out to be negligible.

The one-to-one correspondence between the optical and the

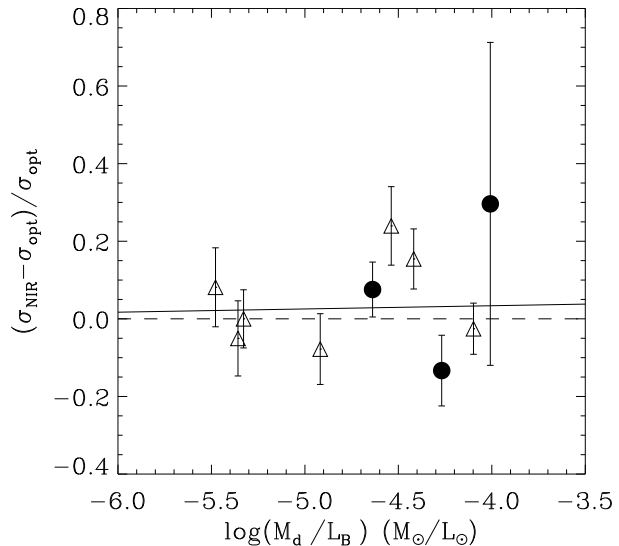


Figure 9. Fractional difference between the infrared and optical dispersions as a function of the ratio of dust mass to B -band luminosity. The solid line is the best fit, given by Eq. 6. The Spearman rank-order correlation coefficient is 0.21 at a significance level of 0.56.

NIR velocity dispersions found for this homogeneous set of early-type galaxies implies that velocity dispersions measured at optical wavelengths are reliable kinematic parameters for early-type galaxies and hence that no bias is introduced in statistical relations that build on such dispersions (such as the $M_{\text{BH}}-\sigma$ relation or the Fundamental Plane). Combined with the simulations by Baes & Dejonghe (2000, 2002), it also supports the traditional point of view on the dust content of early-type galaxies, namely that they are virtually optically thin. While some observational studies hinted towards the existence of a substantial diffuse dust component in early-type galaxies (e.g. Temi et al. 2004, 2007; Leeuw et al. 2004; Vlahakis et al. 2005), the most recent results from the recently launched Herschel Space Observatory indicate a dearth of diffuse dust in the few elliptical galaxies studied so far (Clemens et al. 2010; Baes et al. 2010; Gomez et al. 2010).

Whereas our results support this scenario, we must be careful for two caveats. On the one hand, our results only set limits on the presence of a smooth, diffusely distributed dust component, which one would expect if the dust has an internal origin. If the dust has an external origin, it is not necessarily coincident with the stellar body. An example is the nearby Virgo Cluster elliptical M86, where the dust is clearly related to stripping from a nearby spiral galaxy and is concentrated some 10 kpc to the south-east of the nucleus (Gomez et al. 2010).

On the other hand, the comparison of optical and NIR velocity dispersions might not be the most sensitive way to measure the optical thickness of early-type galaxies. The simulations of Baes & Dejonghe (2000, 2002) indicate an effect of a few percent only for optical depths of order unity. Combined with the measurement errors and other possible effects such as different stellar populations dominating the kinematics at optical and NIR wavelengths, our results should be considered only in a statistical sense and one should take care not to directly interpret results on individual galaxies in terms of optical thickness. A clear example is the case of NGC 1380: in spite of a clear dust lane in optical images (Jordán et al. 2007) and a significant IRAS dust mass of $7.6 \times 10^5 M_{\odot}$, the NIR velocity dispersion is lower than the optical dispersion.

Table 3. IRAS flux densities and dust characteristics.

Galaxy	S(60 μ m) [Jy]	S(100 μ m) [Jy]	log(M_d) [M_\odot]	T_d [K]	log(M_d/L_B) [M_\odot/L_\odot]
NGC 1316	3.070 \pm 0.030	8.110 \pm 1.900	6.11 \pm 0.25	27.2 \pm 2.2	-4.64
NGC 1336	...	0.260 \pm 0.095	4.73	...	-4.54
NGC 1339	0.2298 \pm 0.14	0.670 \pm 0.058	5.09 \pm 0.25	26.5 \pm 2.1	-4.42
NGC 1351	0.090 \pm 0.021	0.510 \pm 0.042	5.41 \pm 0.24	22.4 \pm 1.5	-4.10
NGC 1379	...	0.140 \pm 0.047	4.46	...	-5.33
NGC 1380	1.040 \pm 0.042	3.440 \pm 0.107	5.88 \pm 0.24	25.6 \pm 1.9	-4.27
NGC 1399	...	0.300 \pm 0.082	4.79	...	-5.48
NGC 1404	...	0.270 \pm 0.056	4.75	...	-5.36
IC 2006	0.120 \pm 0.015	0.320 \pm 0.047	4.71 \pm 0.25	27.2 \pm 2.2	-4.92
ESO 358-G59	...	0.380 \pm 0.060	4.90	...	-4.01

A clearer picture on the optical thickness of early-type galaxies will hopefully emerge in the near future when substantial numbers of nearby early-type galaxies will be observed as part of several Herschel Key Programs, including the Herschel Virgo Cluster Survey (Davies et al. 2010) and the Herschel Reference Survey (Boselli et al. 2010).

ACKNOWLEDGMENTS

This research has made use of NASA’s Astrophysics Data System and the NASA/IPAC Extragalactic Database (NED) which is operated by the Jet Propulsion Laboratory, California Institute of Technology, under contract with the National Aeronautics and Space Administration. This research also has made use of the SIMBAD database, operated at CDS, Strasbourg, France. JV acknowledges FWO Vlaanderen for the financial support. AJR was supported by the FONDAP Center for Astrophysics CONICYT 15010003 and by the National Science Foundation grants AST-0808099 and AST-0909237. We also wish to thank the referee for constructive comments on the manuscript.

REFERENCES

Baes M., Clemens M., Xilouris E. M., et al., 2010, *A&A*, 518, L53
 Baes M., Dejonghe H., 2000, *MNRAS*, 313, 153
 Baes M., Dejonghe H., 2001, *ApJ Letters*, 563, L19
 Baes M., Dejonghe H., 2002, *MNRAS*, 335, 441
 Baes M., Dejonghe H., De Rijcke S., 2000, *MNRAS*, 318, 798
 Bender R., Saglia R. P., Gerhard O. E., 1994, *MNRAS*, 269, 785
 Bernardi M., Sheth R. K., Annis J., et al., 2003, *AJ*, 125, 1866
 Boselli A., Eales S., Cortese L., et al., 2010, *PASP*, 122, 261
 Cappellari M., Emsellem E., 2004, *PASP*, 116, 138
 Clemens M. S., Jones A. P., Bressan A., et al., 2010, *A&A*, 518, L50+
 Davies J. I., Baes M., Bendo G. J., et al., 2010, *A&A*, 518, L48
 Desroches L., Quataert E., Ma C., West A. A., 2007, *MNRAS*, 377, 402
 Djorgovski S., Davis M., 1987, *ApJ*, 313, 59
 Dressler A., Lynden-Bell D., Burstein D., et al., 1987, *ApJ*, 313, 42
 Ebner K., Balick B., 1985, *AJ*, 90, 183
 Ferguson H. C., 1989, *AJ*, 98, 367
 Ferrarese L., Merritt D., 2000, *ApJ Letters*, 539, L9

Fraix-Burnet D., Dugué M., Chattopadhyay T., Chattopadhyay A. K., Davoust E., 2010, *MNRAS*, 1098+
 Gaffney N. I., Lester D. F., Doppmann G., 1995, *PASP*, 107, 68
 Gaffney N. I., Lester D. F., Telesco C. M., 1993, *ApJ Letters*, 407, L57
 Gavazzi G., Boselli A., Scodreggio M., Pierini D., Belsole E., 1999, *MNRAS*, 304, 595
 Gebhardt K., Bender R., Bower G., et al., 2000, *ApJ Letters*, 539, L13
 Gomez H. L., Baes M., Cortese L., et al., 2010, *A&A*, 518, L45
 Goudfrooij P., de Jong T., 1995, *A&A*, 298, 784
 Graham A., Colless M., 1997, *MNRAS*, 287, 221
 Graham A. W., 2008, *ApJ*, 680, 143
 Graham A. W., Onken C. A., Athanassoula E., Combes F., 2010, *ArXiv e-prints*
 Gültekin K., Richstone D. O., Gebhardt K., et al., 2009, *ApJ*, 698, 198
 Guzman R., Lucey J. R., Bower R. G., 1993, *MNRAS*, 265, 731
 Hawarden T. G., Longmore A. J., Tritton S. B., Elson R. A. W., Corwin Jr. H. G., 1981, *MNRAS*, 196, 747
 Jordán A., Blakeslee J. P., Côté P., et al., 2007, *ApJS*, 169, 213
 Kormendy J., Bender R., 2009, *ApJ Letters*, 691, L142
 Kuntschner H., 2000, *MNRAS*, 315, 184
 La Barbera F., Lopes P. A. A., de Carvalho R. R., de La Rosa I. G., Berlind A. A., 2010, *MNRAS*, 408, 1361
 Leeuw L. L., Sansom A. E., Robson E. I., Haas M., Kuno N., 2004, *ApJ*, 612, 837
 Lester D. F., Gaffney N. I., 1994, *ApJ Letters*, 431, L13
 Lyubenova M., Kuntschner H., Silva D. R., 2008, *A&A*, 485, 425
 Michard R., 2005, *A&A*, 441, 451
 Michard R., Prugniel P., 2004, *A&A*, 423, 833
 Moorwood A., Cuby J., Biereichel P., et al., 1998, *The Messenger*, 94, 7
 Nowak N., Saglia R. P., Thomas J., et al., 2007, *MNRAS*, 379, 909
 Nowak N., Saglia R. P., Thomas J., Bender R., Davies R. I., Gebhardt K., 2008, *MNRAS*, 391, 1629
 Pahre M. A., Djorgovski S. G., de Carvalho R. R., 1995, *ApJ Letters*, 453, L17
 Pickles A. J., 1998, *PASP*, 110, 863
 Prugniel P., Simien F., 1996, *A&A*, 309, 749
 Ribeiro A. L. B., Dantas C. C., 2010, *A&A*, 521, A58+
 Rothberg B., Fischer J., 2010, *ApJ*, 712, 318
 Silge J. D., Gebhardt K., 2003, *AJ*, 125, 2809
 Silge J. D., Gebhardt K., Bergmann M., Richstone D., 2005, *AJ*, 130, 406

- Silva D. R., Kuntschner H., Lyubenova M., 2008, *ApJ*, 674, 194
Stoehr F., Fraquelli D., Kamp I., et al., 2007, *Space Telescope European Coordinating Facility Newsletter*, 42, 4
Temi P., Brighenti F., Mathews W. G., 2007, *ApJ*, 660, 1215
Temi P., Brighenti F., Mathews W. G., Bregman J. D., 2004, *ApJS*, 151, 237
van der Marel R. P., van Dokkum P. G., 2007, *ApJ*, 668, 756
van Dokkum P. G., Franx M., 1995, *AJ*, 110, 2027
Veron-Cetty M., Veron P., 1988, *A&A*, 204, 28
Vlahakis C., Dunne L., Eales S., 2005, *MNRAS*, 364, 1253
Winge C., Riffel R. A., Storchi-Bergmann T., 2009, *ApJS*, 185, 186
Wise M. W., Silva D. R., 1996, *ApJ*, 461, 155
Wise M. W., Silva D. R., 1997, in *The Nature of Elliptical Galaxies; 2nd Stromlo Symposium*, edited by M. Arnaboldi, G. S. Da Costa, & P. Saha, vol. 116 of *Astronomical Society of the Pacific Conference Series*, 364
Witt A. N., Thronson Jr. H. A., Capuano Jr. J. M., 1992, *ApJ*, 393, 611
Zhu G., Blanton M. R., Moustakas J., 2010, *ApJ*, 722, 491